Aircraft Microphysical Documentation from Cloud Base to Anvils of Hailstorm Feeder Clouds in Argentina

DANIEL ROSENFELD

The Hebrew University of Jerusalem, Jerusalem, Israel

WILLIAM L. WOODLEY

Woodley Weather Consultants, Littleton, Colorado

TERRENCE W. KRAUSS AND VIKTOR MAKITOV

Weather Modification, Inc., Fargo, North Dakota

(Manuscript received 27 February 2005, in final form 21 December 2005)

ABSTRACT

Documentation during January and February 2000 of the structure of severe convective storms in Mendoza, Argentina, with a cloud-physics jet aircraft penetrating the major feeder clouds from cloud base to the −45°C isotherm level is reported. Complementary radar, satellite, and radiosonde measurements are incorporated into the study. The main research goal was the description of the microphysical evolution of the convective feeders of the hailstorms from cloud base to the anvil in an attempt to gain insights into the microphysical evolution of the clouds that are associated with the high frequency of large hail in the region. The aircraft penetrated preferentially the tops of young growing elements, which were typically the major feeders to severe hailstorms, producing hail that is large (>3 cm) in size. Cloud bases typically were at 6°–14°C, with typical base updrafts of 4–7 m s^{-1}. The cloud updrafts increased with height, exceeding 25 m s^{-1} at heights ≥7 km and, on occasion, 40 m s^{-1} at heights >8 km. Thermal buoyancies of 5°–8°C were measured in the convective towers at heights of 8–10 km. The vertical wind shear was weak below 6 km but increased strongly above that level as the west winds cleared the Andes barrier, which averages 6.1 km to the west of Mendoza. The clouds had very little coalescence and contained no detectable precipitation-sized particles >100 μm at temperatures >−15°C. Nearly adiabatic cloud water with most cloud water still not converted into precipitation-sized hydrometeors (>100 μm in diameter) was found in cloud filaments within the strongest updrafts up to the level of homogeneous freezing, reaching 4 g m^{-3} at −38°C in one cloud before vanishing abruptly at colder temperatures. Graupel >1 mm appeared at the tops of growing new towers at temperatures <−27°C, in agreement with radar first-echo heights of about 8 km.

1. Introduction

The province of Mendoza in western Argentina (32°S, 68°W), which is known worldwide for its wine production, is one of the most hail-prone areas of the world. Losses to agriculture as a result of hail are typically 10% of the total annual agricultural production, and on average approximately 20% of the agricultural area receives some hail annually (information was obtained online at http://www.contingencias.mendoza.gov.ar). Because of the economic losses in Mendoza Province from the damaging hail, especially those suffered by the high-value grape crop, seeding for hail suppression has been conducted, with some interruptions, since 1985. The initial efforts employed Russian technology and silver iodide (AgI) rockets, guided by tracking radar, to seed the high-reflectivity cores of incipient hailstorms (Makitov 1999). From 1998 to 2004, it was replaced by an airborne hail suppression project, which was implemented by Weather Modification, Inc., (WMI) of Fargo, North Dakota, for the Ministry of Economy of the government of Mendoza, Argentina.

Besides engaging in operational hail-suppression

Corresponding author address: Prof. Daniel Rosenfeld, Institute of Earth Sciences, The Hebrew University of Jerusalem, Jerusalem 91904, Israel.
E-mail: daniel.rosenfeld@huji.ac.il

seeding, WMI has invested some of its resources over the years in research to increase understanding of hail-producing clouds and their response to seeding intervention. In Argentina this research involved documentation of the dynamical and microphysical structure of the natural and seeded hailstorms during January and February of 2000, using aircraft, radar, and satellite observations. The measurements provided unique in situ cloud-physics data of feeder clouds to severe hailstorms, with coverage from base to the anvil levels. This study uses exclusively the data of the natural (not seeded) clouds to provide insights to the microphysical evolution of the tops of the hailstorm convective elements as they grow from cloud base to the anvil level. The objectives in the context of this goal were the documentation of the vertical evolution of the cloud drop size distribution, cloud liquid water contents (LWC), longevity of the supercooled water, the initiation of precipitation in both liquid and ice processes, and the glaciation temperature, below which no supercooled water is available for the growth of hailstones. Because of the risk of hailstones in the mature cloud elements, the flight emphasis had to be on the tops of young growing elements, which were typically the major feeders to the severe hailstorms already in progress. One ideally would like to ascend with a cloud parcel from cloud base to the anvil level. However, this approach is not practical because most cloud elements lose their identity and the storm complex appears to be built by a succession of cloud towers that take over the new growth with height. The flight strategy was aimed at penetrating the strongest visible well-defined feeders near their top and attempting to keep up with the strongest new growth while avoiding the hazard of large hail falling from above and keeping eye contact with a safe exit from the well-defined cloud tower at the penetration level.

As documented herein, unique measurements were made by the WMI cloud-physics Learjet aircraft down to −45°C in the powerful updrafts of these storms, revealing thermal buoyancies up to 8°C, updrafts >40 m s^{-1}, and occasional cloud volumes of nearly adiabatic water contents to the level of homogeneous freezing within the most intense clouds. Because of the microphysically continental composition of the clouds (i.e., large concentration of small drops with slow coalescence), these strong updrafts carried the condensates in the form of small liquid water cloud droplets (up to 4 g m^{-3}) to near −38°C, which is the temperature of homogeneous freezing. Comparable supercooling has been observed previously in microphysically continental clouds in Texas by Rosenfeld and Woodley (2000) and, to a lesser extent, in premonsoon smoky clouds in Thailand (Andreae et al. 2004).

Other than the measurements in Texas (Rosenfeld and Woodley 2000) and the Argentine observations to be addressed here, little has been measured directly by aircraft previously in the upper portions (i.e., >8 km) of severe convective towers. The lone known exception was the recent use by Heymsfield et al. (2005) of a cloud-physics jet aircraft to penetrate an intense convective core in Florida having an updraft of 25 m s^{-1} at temperatures from −33° to −36°C to document homogeneous ice nucleation in tropical convection and its influence on cirrus anvil microphysics. The amount of supercooled water there peaked at only about 10% adiabatic water, in contrast to the peak of 50% in west Texas (Rosenfeld and Woodley 2000) to the record measurement of nearly 100% adiabatic water in Argentina (this study), respectively. Cloud-physics jet aircraft have been used also to make measurements in thunderstorm anvils (Knollenberg et al. 1982; Smith et al. 1994; Lawson et al. 1998).

At lower altitudes, the armored T-28, which had (this aircraft has been decommissioned) a limited service ceiling of less than 8 km, had been used to make extensive measurements in hailstorms in the United States (Musil et al. 1986, 1991) and in Switzerland (Musil and Smith 1986). In the study by Musil et al. (1986), the armored T-28 traversed a weak-echo region and found a continuous updraft averaging 30 m s^{-1} over a track of 14 km, with a maximum of 50 m s^{-1}. The aircraft was carried from −9° to −30°C by the strong updraft during the traverse. The convective core appeared to be undiluted, having a hot-wire-measured supercooled liquid water content of 6 g m^{-3} and no ice. The maximum echo top was 16 km, and hail up to 4 cm was encountered to the west of the weak-echo region, which was reported to have had droplet concentrations of 600 cm^{-3} and mean droplet diameters <10 μm. [The forward-scattering spectrometer probe (FSSP) apparently undermeasured the cloud droplets, probably because of the icing of the probe, and the signal faded gradually during the penetration.]

2. Climate of Mendoza

The western border of Mendoza is occupied by the main Andean cordillera, with a number of peaks above 6400 m. Climatic conditions are semiarid, and the annual rainfall for the capital city Mendoza, lying 800 m above sea level, is 200 mm. Regional water needs are met by using runoff from snowmelt from the Andes range. The moisture from the Pacific Ocean is blocked by the mountain range. Most of the summer precipita-

tion is produced by convective clouds feeding on tropical and Atlantic Ocean moisture. A study of four hail seasons (i.e., from 15 October to 31 March, in 2000–03 inclusive) revealed that 60% of the days (371 out of 623) had thunderstorms, 18% had hailstorms, and 8% had hailstorms with stones >2 cm. Thus, the storms of the Mendoza region are often severe. The average lifted index (LI) on days with thunderstorms determined from radiosondes released daily at 1600 UTC (1300 local time) at the Cruz Negra radar site was −2.83, and the mean precipitable water was 2.1 cm. Strong instability, a source of moisture from the north and east, great depths of supercooled water, and strong shearing winds aloft provide the necessary (though not always sufficient) ingredients for these hail-producing storms. The Andes range obviously figures into the storm equation, especially with respect to the initiation of the severe nocturnal convection. The mountains are believed to cause a capping inversion due to subsidence flow on the east side of the range, which helps to suppress the premature release of convective instability, but also are thought to provide a mountain–plain diurnal circulation driven by strong surface radiation over the foothills, causing low-level air to converge over the Andes Mountain crests during the daytime and a reverse circulation during the night that creates surface convergence zones and a lifting mechanism for triggering thunderstorms during the evening over the plains. Validating this conjecture requires more research.

The bulk of the summer precipitation comes late in the day and at night. The most frequent time of storm initiation is 1900 UTC (1600 local time). The peak in storm activity occurs near sunset (approximately 0000 UTC, or 2100 local time), and storms lasting past local midnight are a common occurrence. Storm properties were found to be a function of maximum cell-top height. For echoes having maximum heights of 8.5 and 16.5 km, the mean storm durations were 0.43 and 2.3 h, the mean radar-estimated precipitation fluxes were 167 and 1900 $m^3 s^{-1}$, and the mean lifetime rain volumes were 440 and 45 000 kton (1 kton $\equiv 10^3$ m^3), respectively.

3. The cloud-seeding program

a. The hail-suppression conceptual model

The cloud seeding is based on the conceptual model of Alberta (Canada) and Colorado hailstorms that evolved from the experiments and studies of Chisholm (1970), Chisholm and Renick (1972), Marwitz (1972a,b,c), Barge and Bergwall (1976), Krauss and Marwitz (1984), and English (1986). Direct observational evidence from the instrumented aircraft penetrations of Colorado and Alberta storms in the 1970s and early 1980s indicates that hail embryos grow within the time-evolving "main" updraft of single-cell storms and within the updrafts of developing "feeder clouds" or cumulus towers that flank mature "multicell" and "supercell" storms (see, e.g., Foote 1984; Krauss and Marwitz 1984).

The growth to large hail is hypothesized to occur primarily along the edges of the main storm updraft where the merging feeder clouds interact with the main storm updraft (Foote 1985; World Meteorological Organization 1995). The mature hailstorm may consist of complicated airflow patterns and particle trajectories; therefore, the cloud seeding cannot hope to affect all embryo sources but attempts to modify the primary hail formation process. In other words, the cloud seeding cannot attempt to eliminate all of the hail but can reduce the size and amount of hail.

b. Time frame and layout

The operational seeding period is from 15 October to 1 April. The project area covers the three Argentine agricultural oases of Mendoza–San Martin in the north, Tunuyan in the center, and San Rafael in the south. A map of Mendoza Province, showing the target fertile agricultural zones (referred to as oases) and the predominant storm generation zones and most frequent storm tracks as determined from analysis of the Cruz Negra radar data is shown in Fig. 1.

c. Resources

1) ATMOSPHERIC SOUNDINGS

A Vaisala, Inc., GPS RS80 radiosonde system was operated at the Cruz Negra radar site (33.447°S, 68.967°W, elevation 915 m MSL). Radiosondes were launched daily at 1600 UTC (1300 local time), especially for supporting the seeding operations. The modified soundings for the two prime days selected for intensive analysis (i.e., 1 and 7 February 2000) are provided in Figs. 2 and 3. In the soundings, the observed surface temperature and dewpoint conditions were modified and mixed throughout the subcloud layer to match the cloud-base height that was observed by the research aircraft.

The two soundings are similar in that the convective condensation level–predicted clouds' bases are relatively high (3000 m MSL, approximately 2100 m AGL) and cool (near +10°C) and the winds are light at low levels and change to westerly above 600 hPa, reaching more than 40 m s^{-1} at the upper levels. Both soundings are unstable, with the sounding for 7 February 2004

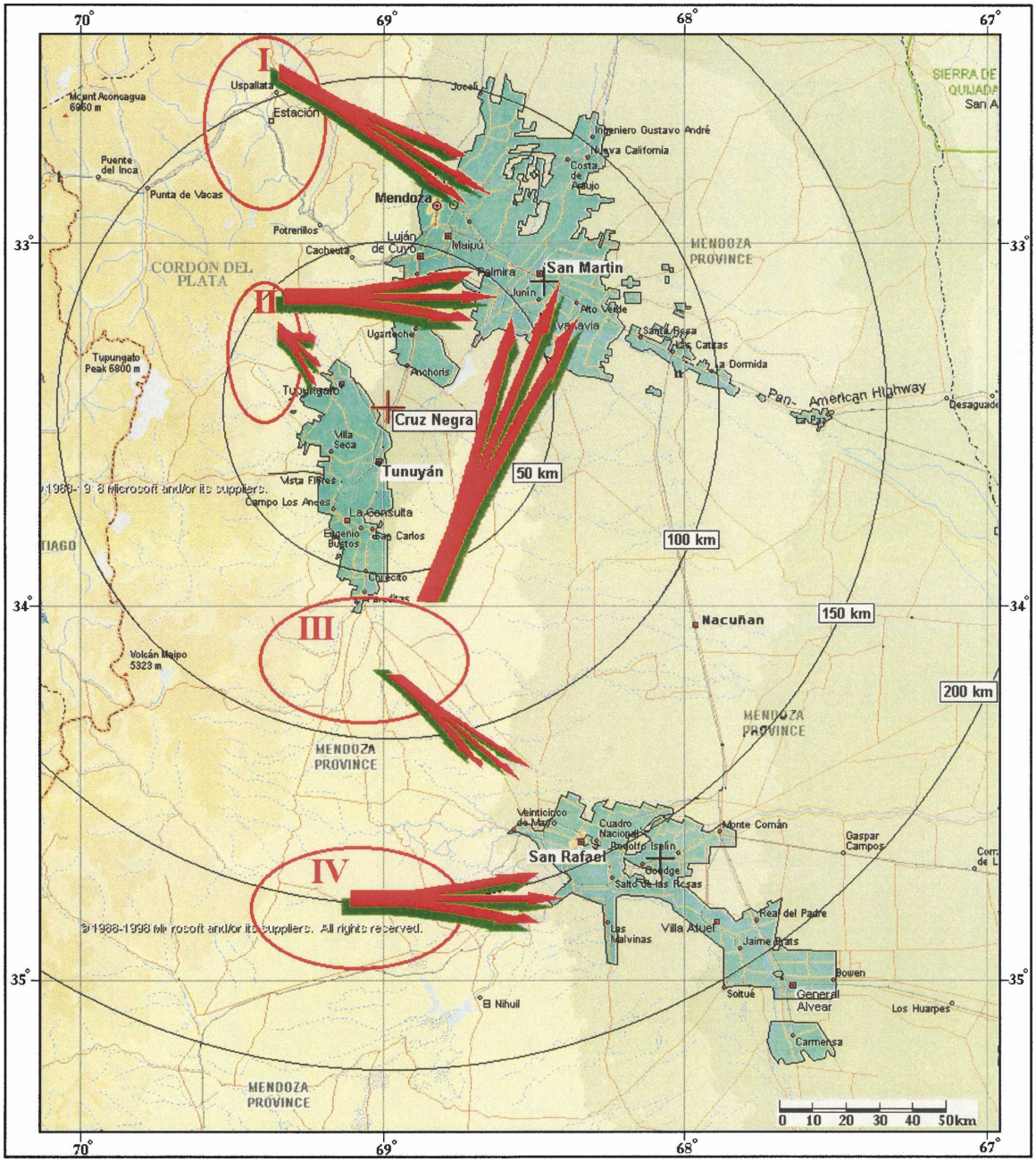

FIG. 1. Map of Mendoza region showing the three fertile agricultural regions, called oases, and the predominant storm tracks and genesis regions as determined from radar data collected at Cruz Negra.

being the more unstable of the two with an LI value of −6.6 and a CAPE of +2209 J kg^{-1}. This instability in conjunction with the shearing winds makes both days ripe for the hail that was observed.

2) PROJECT RADAR SYSTEMS

The project radar is a WR-100 Enterprise Electronics Corporation (EEC) C-band radar system mounted on a 10-m tower at Cruz Negra. The radar was operated 24 h day^{-1} during the operational period. A complete volume scan was performed every 4.2 min.

A software package called Thunderstorm, Identification, Tracking, Analysis, and Nowcasting (TITAN) was added to the radar. TITAN is a software system that ingests radar data, converts it into Cartesian coordinates, identifies storms, tracks them, and displays the tracks and forecasts (Dixon and Wiener 1993).

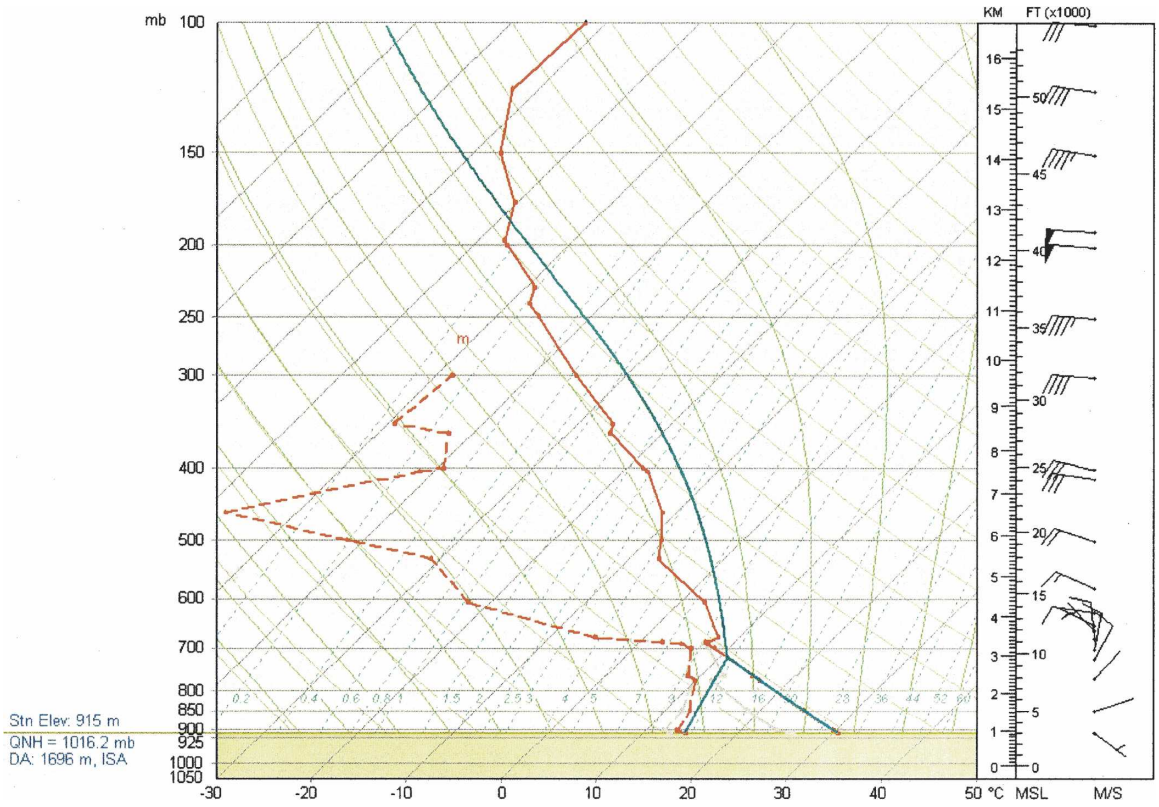

FIG. 2. Atmospheric sounding taken at 1300 LT (LT = UTC − 3 h) at the Cruz Negra radar site in Mendoza on 1 Feb 2000. The temperature and humidity trace for a parcel lifted adiabatically from the surface with a temperature of 30.5°C and dewpoint of 14.5°C is also indicated, producing a cloud base near the observed values of 11°C at 2.8 km MSL.

4. Aircraft cloud-physics measurements

a. Aircraft

The WMI Learjet Model 35A was configured for cloud-physics measurements during January and February of 2000. In addition to its seeding capability of 408 ejectable 20-g AgI flares, the Learjet was equipped with an FSSP-100 probe for sizing particles in the range of 2–44 μm and an optical array probe (OAP)–2D cloud (2DC) probe for imaging particles in the range of 25–800 μm. In addition, the aircraft had a Droplet Measurement Technologies (DMT) hot-wire instrument to measure liquid water contents, temperature and dewpoint probes, a Ball variometer for the inference of cloud drafts, and a forward-looking camera with viewing through the upper-left portion of the copilot's windshield.

All data from the Learjet were recorded using a Science Engineering Associates (SEA) Model M300 data acquisition system. Ground calibrations and comparisons with radiosondes were conducted for checks of accuracy for state parameters. A Setra S270 static pressure transducer provided pressure altitude measurements. A Setra S239 differential pressure transducer provided measurements of airspeed. Temperature was obtained using a Rosemount Model 102 de-iced platinum resistance–type total temperature sensor capable of measuring temperatures from −50° to +50°C, with an accuracy of ±0.5°C and a response constant of 1 s. The dewpoint temperature was obtained using a General Eastern GE11B optical dewpoint system. Accuracy is stated by the manufacturer to be ±0.25°C, and the response time is quoted as 1°C s^{-1}, limited by the maximum mirror cooling rate. A DMT LWC-100 was used to measure liquid water concentrations from 0 to 5 g m^{-3} with an accuracy of ±0.2 g m^{-3} and a response time of 50 ms (spatial resolution of ~2 m). The Ball Variometer BV4.0 is a transducer that measures the vertical velocity of the aircraft up to 4000 ft min^{-1} (20 m s^{-1}). The BV4.0 is interfaced with the aircraft pitot–static system.

b. Measurements of the drop size distribution (DSD)

The DSD was measured using the FSSP-100 instrument, measuring drops in 15 size bins between 2 and 44 μm. The instrument sizing calibration was validated to

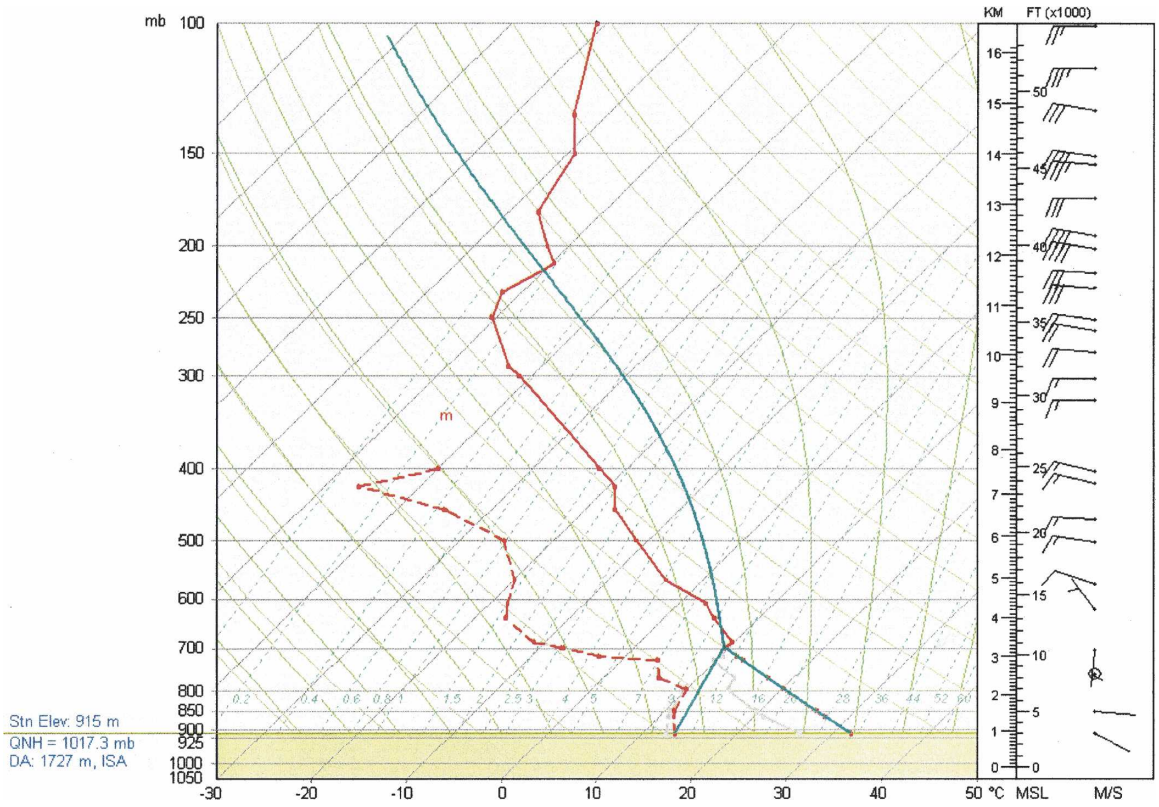

FIG. 3. Atmospheric sounding taken at 1300 LT (LT = UTC − 3 h) at the Cruz Negra radar site in Mendoza on 7 Feb 2000. The temperature and humidity trace for a parcel lifted adiabatically from the surface with a temperature of 32°C and dewpoint of 13.5°C is also indicated, producing a cloud base near the observed values of 9.7°C at 3.1 km MSL.

be correct, using glass beads. Correction for activity dead time was applied. Even after this correction, the FSSP grossly underestimated the integrated LWC with respect to the DMT hot-wire water. This can occur in part as a result of the FSSP operating at true airspeeds (TAS) in excess of 160 m s^{-1}, whereas the maximum operating TAS of the FSSP is 100 m s^{-1}. Beyond that velocity the relative slow response of the electronics translates the increased transit velocity of a particle into a reduced particle size (Baumgardner and Spowart 1990). The extent of the dependence of cloud drop size on TAS can be estimated a posteriori by relying on the assumption that cloud droplet effective diameter remains nearly constant at a fixed height above cloud base (Freud et al. 2005). Suitable measurements of cloud drops at the same altitude at sufficiently variable TAS were available from the flight of 1 February 2000. Data from narrow ranges of 2°C intervals of isotherm heights were analyzed. One-second flight data were selected if 2DC probe counted less than 1 SHADOR (SHADOR is the term for any shadow of particle that is greater than or equal to two 25-μm image elements) particle and the nominal droplet concentration was greater than 10 cm^{-3}. Based on the result, shown in Fig. 4, 0.73 (TAS − 107) μm was added to the FSSP-measured drop diameters. The application of this drop size correction increased the integrated FSSP water by 30%–40%, but there was still a remaining underestimate of the LWC by a factor of about 10, as is evident from Fig. 5.

The remaining discrepancy by a factor of 10 can be explained by misalignment of the optics, which causes a reduced sample volume. The consistency of the data during the flights rules out problems such as fogging or wetting of the optics. The DMT LWC was taken as the more believable reference, and the FSSP readings after activity correction of the drop concentration and TAS correction of the drop diameter were multiplied by the large factor of 10 for the whole FSSP measurement campaign of 27 January–8 February 2000. The relation as presented in Fig. 5 shows useful relations on which the FSSP can be adjusted. Although misalignment of the optics is suspected, why such a large adjustment of the FSSP values was needed to bring them into agreement with the DMT values is unknown, and it cannot be traced back because the specific FSSP instrument is no longer available. Therefore, some ambiguity between the drop size and concentrations remains. Ac-

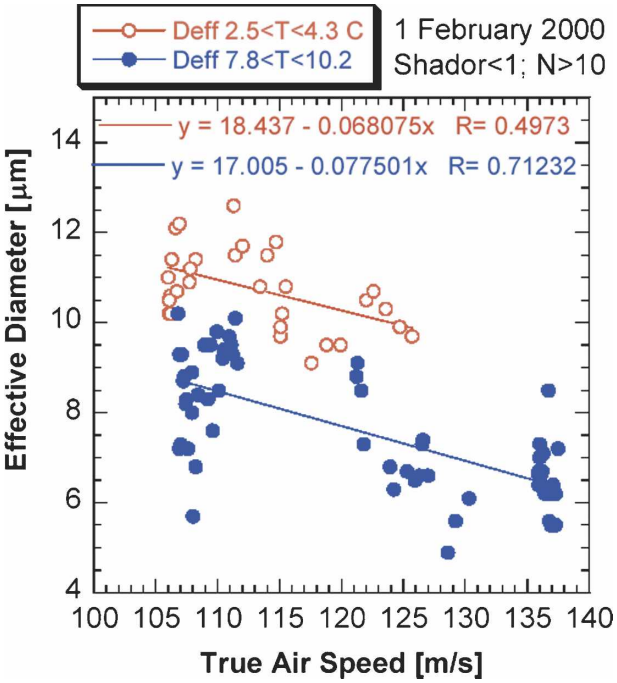

FIG. 4. The dependence of cloud drop effective diameter on the true airspeed at two narrow height ranges, as measured in the convective storms of 1 Feb 2000. Each point represents 1 s of flight path.

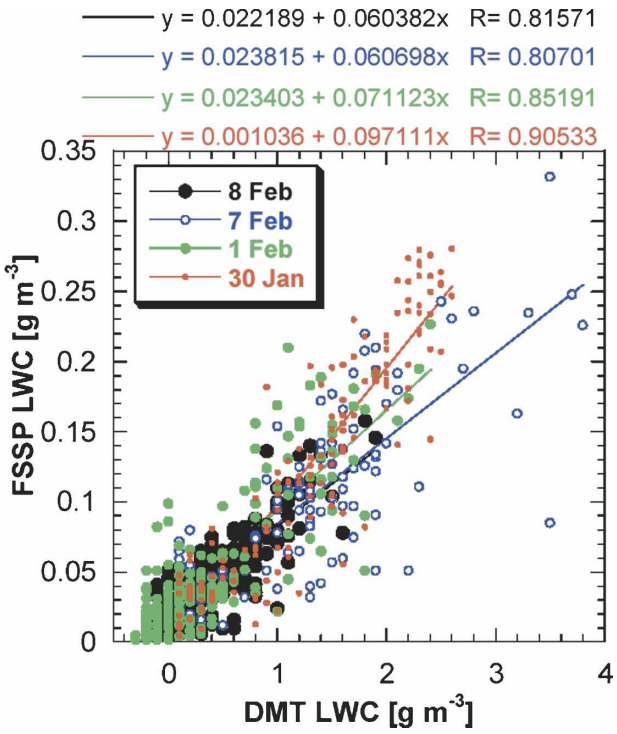

FIG. 5. The relation between FSSP and DMT hot-wire-measured LWC, after the activity and TAS corrections were applied to the FSSP data. Data from four days are presented. The comparison is done for all data points that had more than 14 uncorrected cloud drops per cubic centimeter and less than 1 2DC count per liter. Where 2DC is not available for the SHADOR rejection criterion, data at $T < -10$°C were not included.

cording to Fig. 4, the error in drop average effective diameter is probably less than 2 μm, which translates to a factor of less than 1.5 in the average drop concentrations.

c. *Evolution of the DSD with height*

The DSD evolution was measured by penetrating the most vigorous cloud elements that could be found at any height, from cloud base to the −45°C isotherm level. The clouds were typically the feeders of the main convective storms, often while merging with the main storm. On occasion, the cores of the main storms were penetrated, as was evident from the strong updrafts (>40 m s^{-1}) that were penetrated and by an eventual encounter with giant hail on 8 February 2000 that forced the end of the measurement campaign.

A complete base-to-top microphysical documentation of the clouds with both the FSSP and DMT hot-wire LWC was obtained for 1 and 7 February 2000. The 2DC instrument was also operative on 1 February, but not for later dates. Measurements were made also on 27, 28, and 30 January but without complete vertical documentation. Clouds with occasional nearly adiabatic updrafts were measured on both 1 and 7 February, as was evident by the peak values of nearly adiabatic LWC measured to the level of homogeneous freezing at −38°C (see Fig. 6), the strong updrafts, and the large thermal buoyancies (see section 5). The amount of highly supercooled water reaching the homogeneous freezing level well exceeded those reported previously in west Texas (Rosenfeld and Woodley 2000).

The vertical evolution of cloud DSD in the intense updrafts of severe hailstorms that occurred on these two days was obtained for the whole vertical span between cloud base and the anvil level (Figs. 7a,b). The cloud DSD had an extremely narrow spectrum width near cloud base. The spectra widened with height but did not start producing a precipitation echo below 8 km. It was shown that single-particle optical counters like the FSSP artificially broaden particle spectra (Baumgardner and Spowart 1990). Therefore, true width of the distribution might be even narrower. To mitigate to the extent possible the impact of droplet spectra broadening on the vertical evolution of the spectra, it is most prudent to concentrate on the drop diameter of the maximum LWC in a volume-weighted cloud DSD. This is defined as the drop size modal LWC, or D_L. This property was used previously to track the vertical evo-

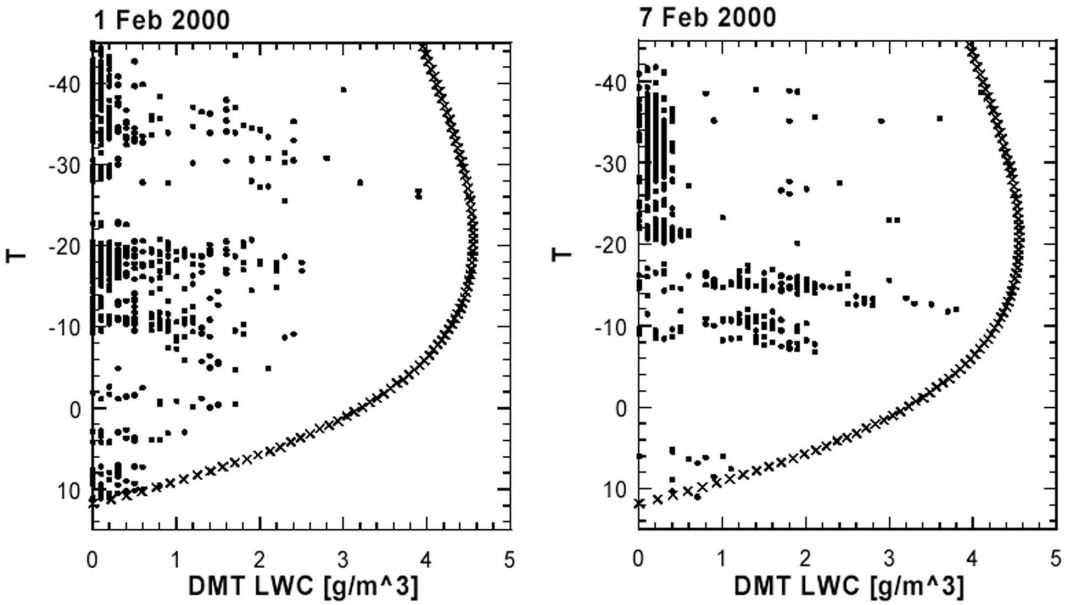

FIG. 6. Distribution of liquid water content as a function of height for the full two flights on (left) 1 and (right) 7 Feb 2000. Each point is 1 s of flight path, measured by the DMT hot-wire instrument. Note the occasional occurrence of very large values up to just below the level of the −40°C isotherm, where the abrupt decrease indicates the occurrence of homogeneous freezing. The tracked line represents the adiabatic water content. Some of the water contents at temperatures ≤−40°C may be due to time lags between the T and LWC sensors.

lution of the main peak of the DSD in convective clouds in a large variety of cloud conditions (Andreae et al. 2004). To put our measurements in global context, the height dependence of D_L was obtained from Fig. 7 and was compared in Fig. 8 with similar measurements that have been made elsewhere with similar probes in a wide range of microphysical regimes (Andreae et al. 2004). Measurements of the vertical evolution of D_L elsewhere showed that the onset of warm rain occurs when D_L exceeds the threshold of 24 μm. Warm rain can occur also at highly supercooled temperatures, but the raindrops freeze readily and collect preferentially the larger cloud drops, as is evident in the monsoon clouds of Thailand (Fig. 8). The DSD in the Argentine hail clouds widened with height all the way to the homogeneous freezing level but barely reached the 24-μm warm rain threshold below the homogeneous freezing level. The relations between effective diameter D_{eff} and D_L (Fig. 9) show a similar indication from D_{eff} reaching 21–22 μm at these heights. Freud et al. (2005) have shown, using a similar FSSP, that these D_{eff} are the values above which significant coalescence and warm rain occurs. These results are robust, because D_{eff} shows much smaller variability (see Figs. 10–12) than the number concentrations and LWC (Tsonis et al. 1987; Freud et al. 2005).

This result suggests that widening of the basic droplet spectrum by coalescence did not play an important role in creating precipitation embryos in these Argentine clouds, except for the highest parts of the supercooled regions. However, it does not exclude the possibility that giant cloud condensation nuclei (CCN) could have still created isolated raindrops that were too sparse to be observed. According to Fig. 8, the coalescence at a given depth above cloud base was as suppressed as in the smoky clouds in the Amazon but was less suppressed than in the "pyro" clouds (i.e., clouds feeding directly on the heat and smoke of fires) there. It appears that excessively large CCN concentrations have the same effect on cloud microstructure and precipitation-forming processes as do strong updrafts in a microphysically continental atmosphere. Indeed, the smoky clouds in the Amazon produced hail up to 2 cm in diameter on the ground in the tropical rain forest (Andreae et al. 2004). It appears that the strength of the updrafts and the concentrations of small CCN have similar effects on cloud microstructure, and the respective contributions of the two factors to an observed cloud profile cannot be easily disentangled.

d. Documentation of individual cloud passes

Base-to-anvil sequences of cloud passes are presented in Figs. 11 and 12 for the 1 and 7 February 2000 cases of large (i.e., >3 cm) hail, respectively. The most vigorous passes were selected for the vertical profiles shown in Figs. 11 and 12. The DSD spectra of the cloud

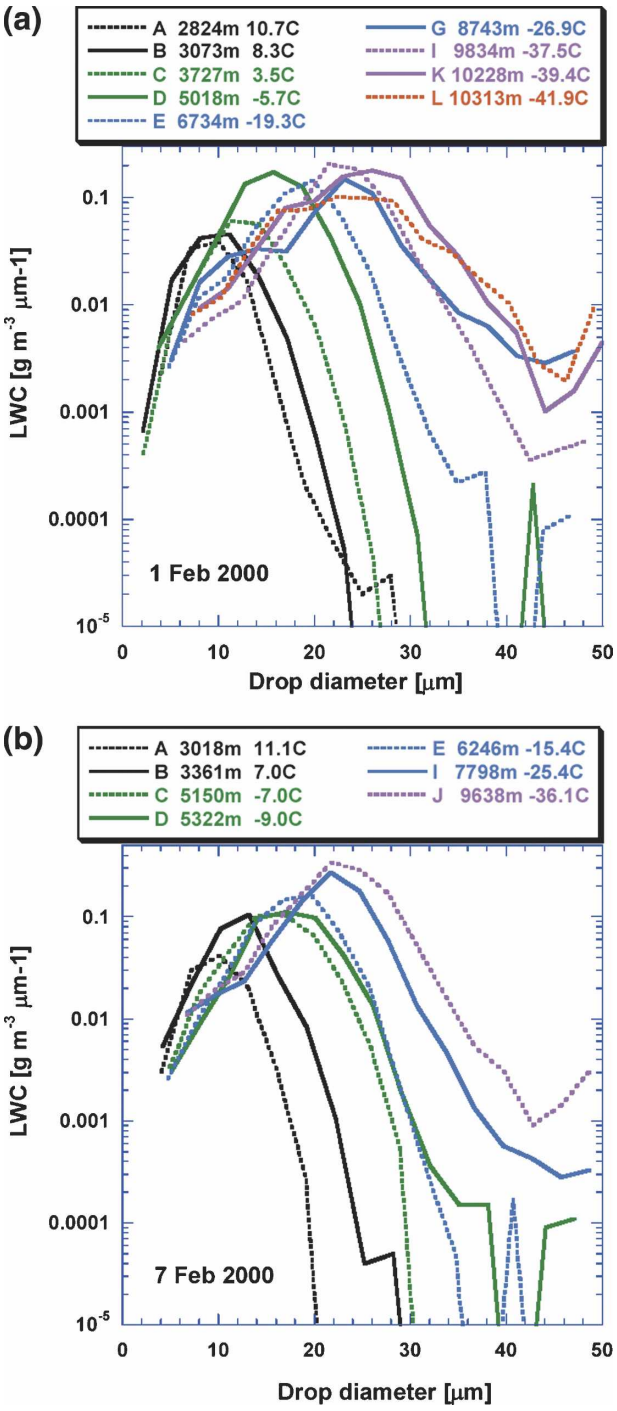

FIG. 7. Vertical evolution of the FSSP-measured cloud DSD from cloud base to the height of homogeneous freezing in the feeders of severe hailstorms in Mendoza on (a) 1 and (b) 7 Feb 2000. The most vigorous cloud element that was encountered at each altitude was selected for this composite, as quantified mainly by the maximum amount of liquid water content. For minimizing the artifacts of hydrometerors on the measured cloud DSD, only 1-s data with FSSP droplet concentrations >500 cm^{-3} were averaged to form the displayed spectra. Obviously, spectrum L in (a) is already of a glaciated cloud, probably composed mainly of frozen cloud drops.

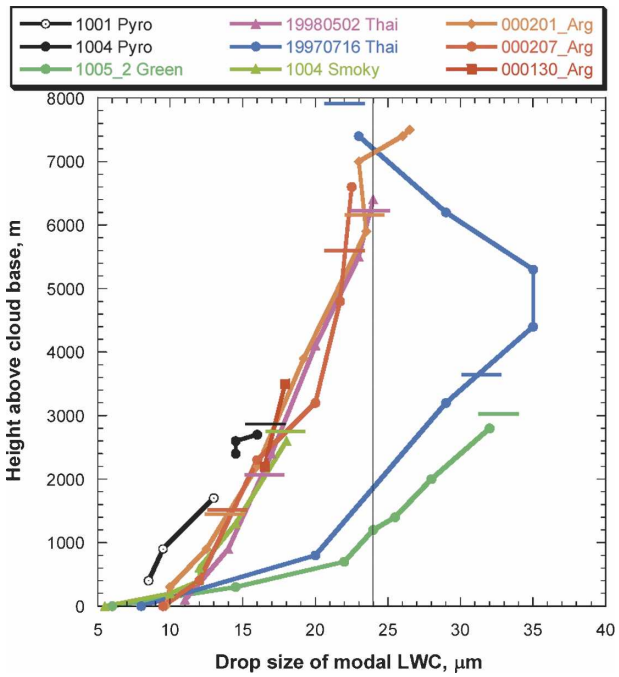

FIG. 8. The dependence of the drop size modal LWC D_L on height above cloud base and temperature, for Argentina hailstorms (red and orange), pyro clouds in the Amazon (black), smoky clouds in the Amazon (light green), smoky clouds in Thailand (pink), monsoon smoke-free clouds in Thailand (blue), and pristine clouds in the Amazon (green). The lower and upper horizontal bars represent the 0° and −30°C isotherm cloud depths. The vertical line at $D_L = 24$ μm represents the warm rain threshold. The Argentina curves are from this study. The rest are from Andreae et al. (2004).

passes are displayed in Figs. 7a and 7b, respectively, labeled with the same panel lettering as found in Figs. 11 and 12 (A, B, etc.).

This is the first time that such results have been reported. Therefore, the full vertical documentation of cloud microstructure on the two days is provided for the benefit of future research and especially for the validation of model simulations. The time reference on the abscissa of each plot is in seconds referenced to UTC midnight (i.e., time t in seconds after UTC midnight = hour × 3600 + minute × 60 + seconds). The presented measurements are temperature (°C), DMT hot-wire liquid water content (g m^{-3}), adjusted FSSP liquid water content (g m^{-3}), particle number concentrations (2–44-μm nominal diameters) as measured by the adjusted FSSP (cm^{-3}, divided by 1000 to fit the right scale), D_{eff} of the FSSP-measured particles (divided by 10 to fit the right scale), and rate of ascent as measured by the Ball variometer. Note that the time scale may change from panel to panel to accommodate the individual cloud passes.

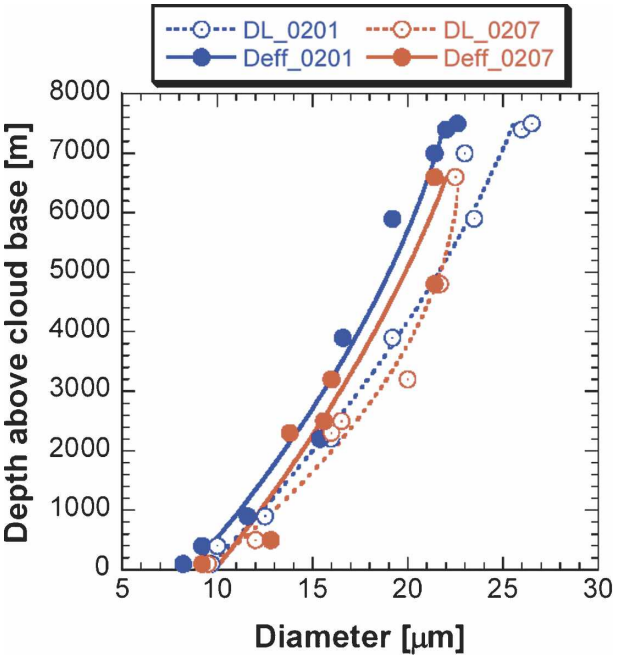

FIG. 9. The relations between D_{eff} and D_L for the droplet spectra plotted in Fig. 7.

The cloud liquid water content increased as expected from cloud base upward up to the homogeneous freezing isotherm of −38°C (see Figs. 11H, I, and J and 12J) in what appear to be nearly adiabatic cloud filaments. The maximum thermal buoyancy was approximately 8°C on both days (see Figs. 11H, J, K, and L and 12J) at the heights of 9–10 km. The expected thermal buoyancy from the radiosonde sounding on 1 February 2000 at 9 km MSL was approximately 5°C (Fig. 2). The atmosphere cooled at the upper levels during the day on 1 February 2000; therefore, the larger thermal buoyancies observed within the storm are not unexpected on this day. The expected thermal buoyancy from the radiosonde sounding on 7 February 2000 at 9 km MSL was approximately 10°C (Fig. 3), which is consistent with the measurements on this day. Cloud water vanished promptly at −38°C, whereas the large thermal buoyancy remained. Of interest is that the FSSP LWC showed little change where the hot-wire DMT LWC responded strongly to what appears to be homogeneous freezing. This is evident best in Fig. 11J, followed by Figs. 11H and 11L. This suggests that the FSSP reacted to the homogeneously frozen cloud drops as if they were cloud droplets, measuring equivalent water content of a little more than one-half of the LWC that occurred in the liquid counterpart of the cloud. This kind of underestimate is to be expected because of the loss of particle sphericity and the change of their refractive index upon freezing.

Updraft velocities were crudely estimated by the rate of ascent of the aircraft, using the Ball variometer, while the pilot maintained constant aircraft attitude and settings prior to cloud penetration. This was difficult to do in the highly turbulent convective elements.

The convective core penetrated during the pass shown in Figs. 12G and 12H was hidden inside a large pileus cloud (such capping clouds were typical on both 1 and 7 February 2000). All that could be seen before penetration was the impressive pileus that was being pushed by the shrouded tower from below. The pileus was penetrated at t = 70 435, and the traverse was very smooth, without discernible turbulence, although the aircraft was carried upward at a rate of about 5 m s^{-1} (1000 ft min^{-1}). At t = 70 450, the aircraft hit the full force of the convective core that was pushing this extensive pileus. The Learjet stalled but control was regained immediately by a couplet of nose-down–nose-up maneuvers that scrambled all that was not tied down in the airplane cabin. The exit from the turbulent convective tower came suddenly at t = 70 462 and was associated with a strong momentary negative-gravity force ("G force"). Once again, all of the loose items hit the aircraft ceiling. The exit was into the other side of the pileus for a duration of another 18 s, where the flight again was very smooth in the updraft of 5 m s^{-1}.

The microstructure of the pileus cloud was clearly different from the convective element, because its cloud base was much higher than that of the convective element that pushed it. Therefore, the LWC was much smaller, cloud droplet concentrations were smaller, and the effective radius of the pileus cloud matter was distinctly smaller (see Fig. 12G). These observations can be generalized to the differences between elevated layer clouds that are not generated by detrainment of convective cloud matter and convective clouds. This principle has been used by Rosenfeld and Lensky (1998) for separating convective and layer clouds by their satellite-retrieved effective radius of cloud drops. These in situ measurements provide support for that method.

The trace of the Ball variometer in Fig. 12H shows clearly the violent excursions of the rate of ascent within the convective element versus the smooth flight in the pileus. One cannot take the draft magnitudes seriously, however, because of the stall of the aircraft and the violent maneuvers that were necessary to maintain its control. Similar stalls occurred several times at the 9–10-km level while penetrating the most vigorous clouds. The Ball variometer unfortunately froze at those altitudes. It was possible to determine, however, that the updraft velocities likely exceeded 35 m s^{-1} in several instances. In the cloud pass shown in Fig. 12H, the Learjet penetrated the pileus and then the con-

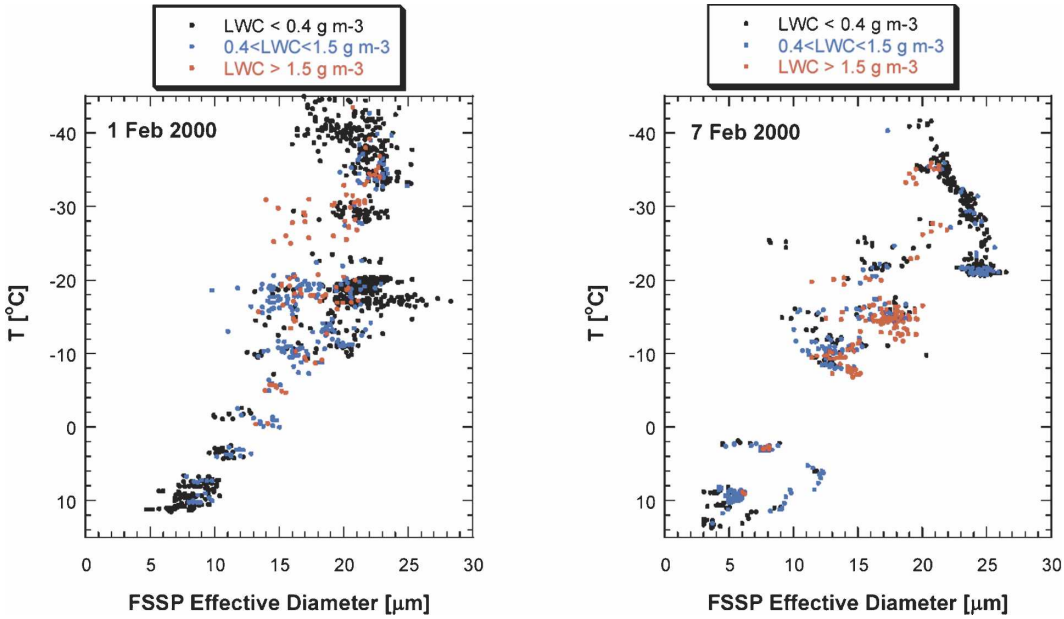

FIG. 10. The dependence of FSSP-measured cloud particle effective diameter on cloud temperature T for cloud passes made on (left) 1 and (right) 7 Feb 2000. Each point represents 1 s of flight path, colored according to the DMT hot-wire liquid water content. All the measurements that include >100 FSSP adjusted counts are presented.

vective core. The aircraft stalled momentarily upon hitting the updraft, despite flying at a true airspeed of 150 m s^{-1} and an angle of attack of 5.7°. According to the illustration in Fig. 13, the updraft velocity determines the angle of attack of the wing with respect to the airflow at the moment the aircraft hit the updraft. A stall occurs when the angle of attack increases beyond a critical value of 17°, at which the flow separates from the upper surface of the wing (in the Learjet a sensor of the angle of attack preempts the aerodynamic stall by mechanically lowering the nose of the aircraft when the angle of attack reaches 17°). According to Fig. 13, the vertical component of the airflow under these conditions is $\overline{OB}$ tan(∠COB), or 150 tan(11.3) = 30 m s^{-1}. This relative updraft estimate starts from the baseline of already existent rising motion outside the convective element of about 5 m s^{-1}, as evident by the existence of the pileus cloud. This brings the lower bound of the updraft to about 35 m s^{-1}. Stalls under similar aerodynamic conditions occurred several other times in violent convective feeders of the hailstorms.

Indications of the vigor of the updrafts were obtained also by other means. During the cloud penetration in Fig. 12J, the aircraft gained an altitude of 540 m during 40 s while maintaining horizontal attitude. This gives a mean updraft of 13.5 m s^{-1}. During the 10-s period of t = 68 321–68 331 the aircraft had an average rate of ascent of 31 m s^{-1}. The peak value of 42.5 m s^{-1} occurred between t = 68 322 and 68 324, which is coincident with the peak buoyancy (temperature) in the cloud (see Fig. 12J). This time is also the exact one at which the DMT hot-wire broke, probably as a result of impact with a hailstone. These updraft velocities are still smaller than the 66 m s^{-1} estimated at the equilibrium level of 11.7 km MSL from the simple relationship $W_{max} = (2 \times \text{CAPE})^{0.5}$ for an adiabatic parcel on 7 February 2000. The equilibrium level is the temperature at which the adiabatic parcel temperature is equal to the environmental temperature at the top of its ascent. The sounding in Fig. 3 gives it as 11.7 km MSL on 7 February and 11.4 km MSL on 1 February (Fig. 2).

The violent updrafts were driven by huge thermal buoyancies of up to 8°C. The updrafts contained cloud filaments of nearly adiabatic water to the level of homogeneous freezing. To document the cloud properties in these updrafts just above the level of homogeneous freezing, where the cloud was expected to consist of homogeneously frozen drops, the aircraft penetrated the top of a vigorously growing cloud at an ambient temperature of −45°C. LWC of up to 0.5 g m^{-3} was found in the cloud (Fig. 11L) at a maximum in-cloud temperature of −37°C. The maximum hot-wire LWC measured in the most vigorous clouds colder than −38°C did not exceed 0.3 g m^{-3} because of the cloud ice. Therefore, a reading of 0.5 g m^{-3} indicates that this cloud contained some liquid water at −37°C. Ice hydrometeors can grow very fast in these highly supercooled water-laden clouds with such strong updrafts,

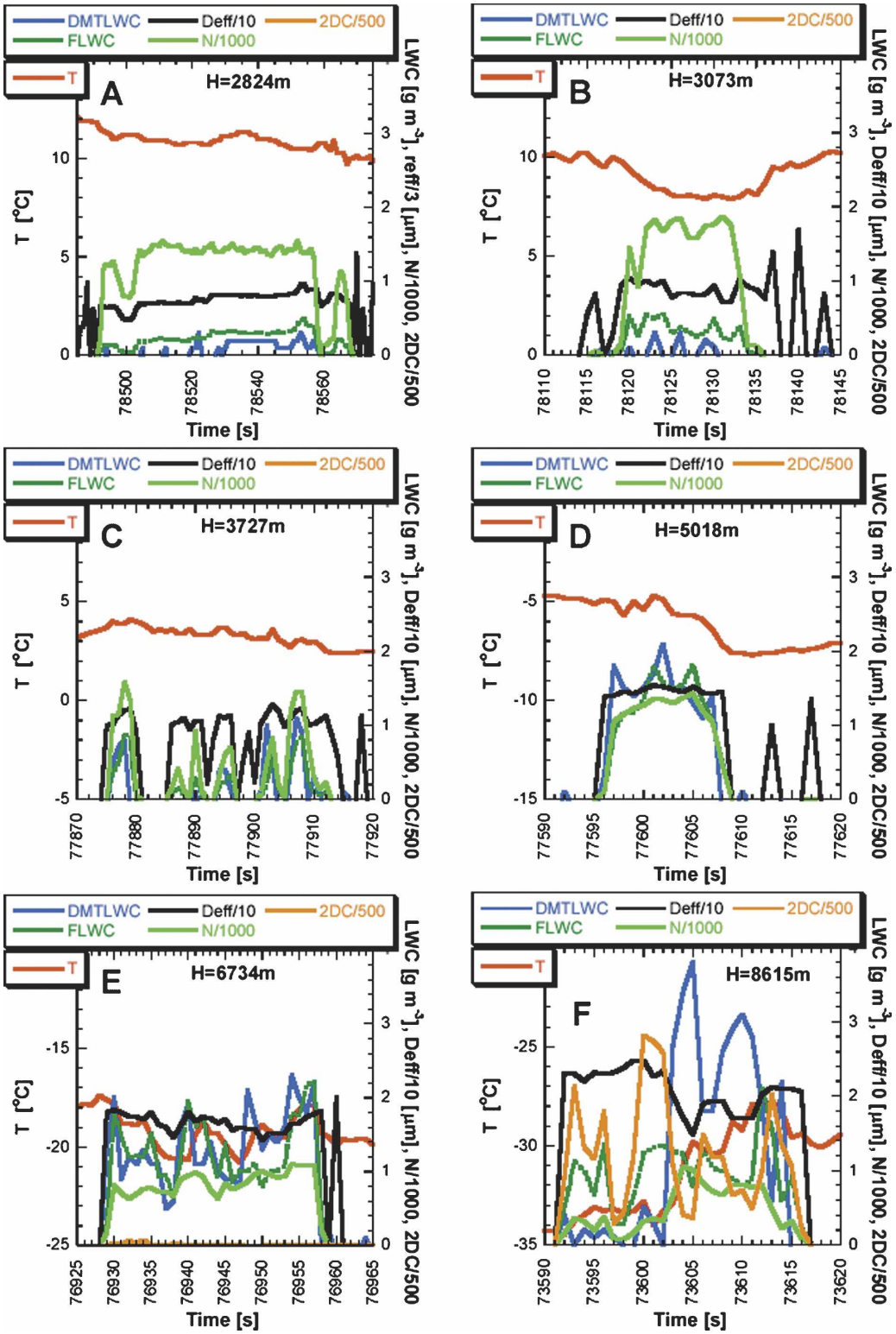

FIG. 11. Cross sections of convective elements of severe hailstorms or in their vicinity on 1 Feb 2000 over Mendoza as measured by the WMI Learjet. The penetrations are in vigorously growing convective elements from cloud base to above the level of homogeneous freezing. The presented measurements are temperature (°C), DMT hot-wire liquid water content (g m^{-3}), adjusted FSSP liquid water content (g m^{-3}), particle number concentrations (2–44 μm in diameter) as measured by the adjusted FSSP (cm^{-3}, divided by 1000 to fit the right scale), and effective diameter D_{eff} of the FSSP-measured particles, divided by 2 to fit the right scale. The abscissa is in seconds from 0000 UTC. Note that the time scale may change from panel to panel to accommodate the individual cloud passes.

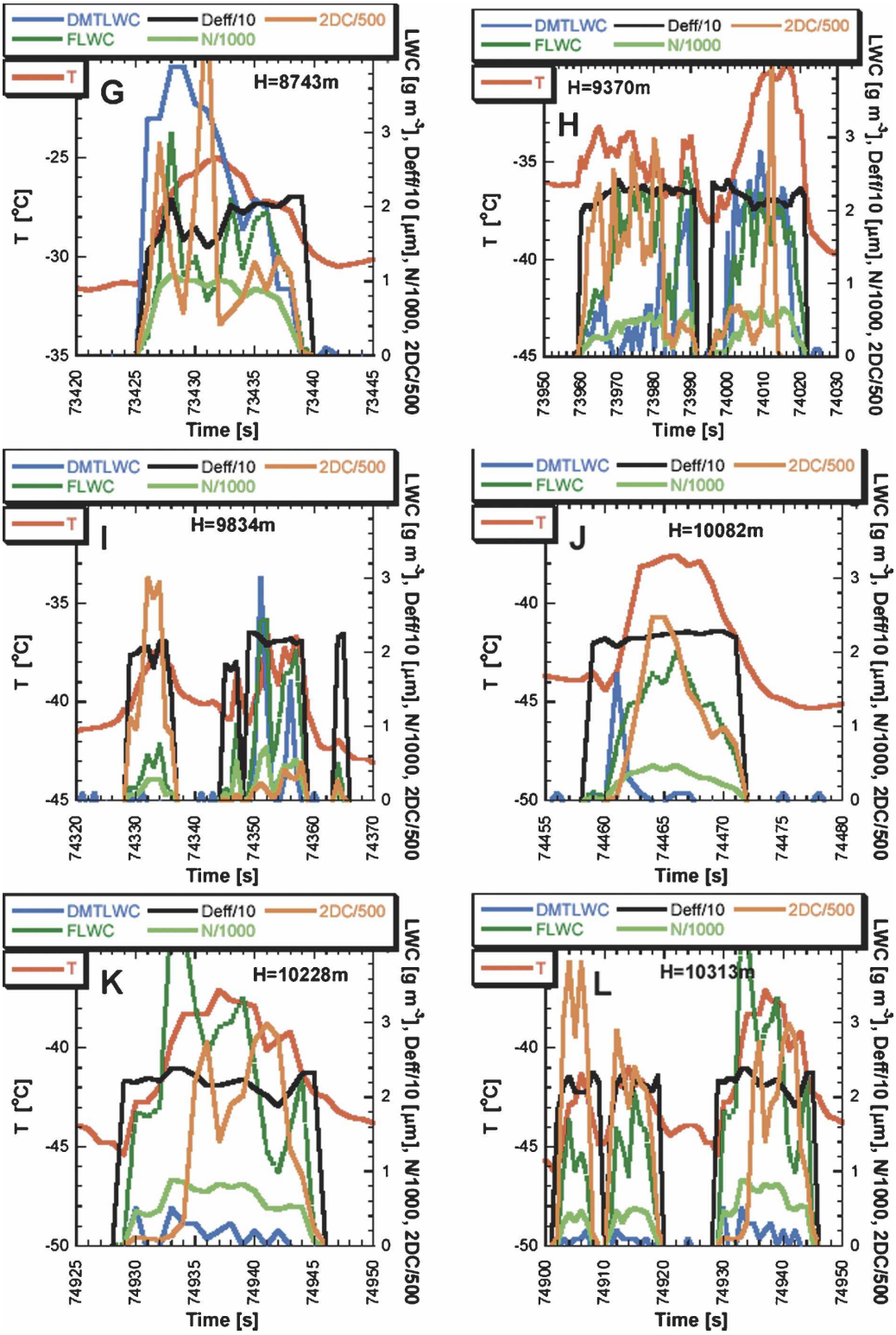

FIG. 11. (*Continued*)

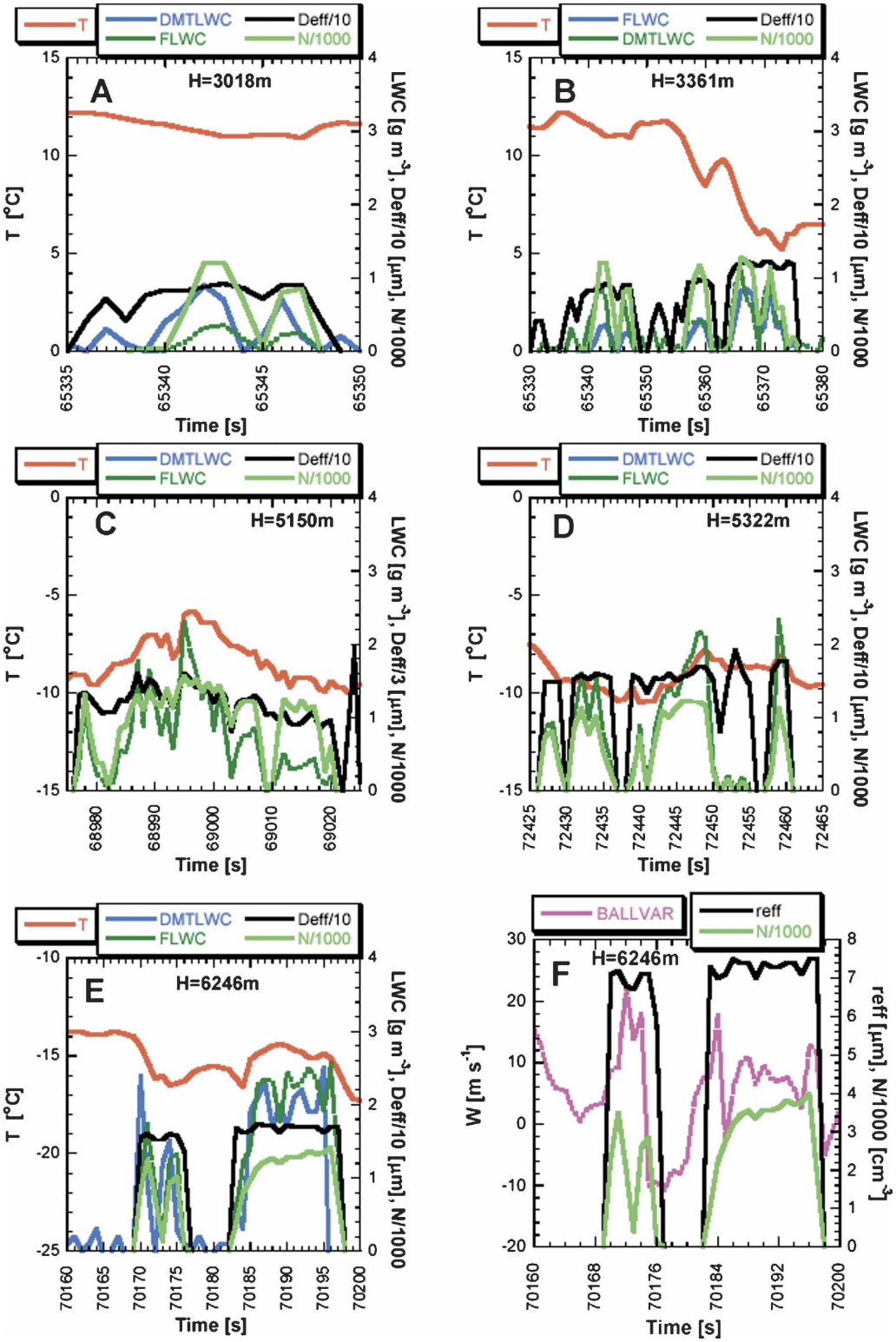

FIG. 12. Same as for Fig. 11, but for 7 Feb 2000. Panels (H) and (F) also show the rate of aircraft ascent, as measured by the Ball variometer. The hot-wire of the DMT LWC probe broke in the middle of the penetration shown in (J). It was not operative in (C), (D), and (G). The 2DC was not operative on this day.

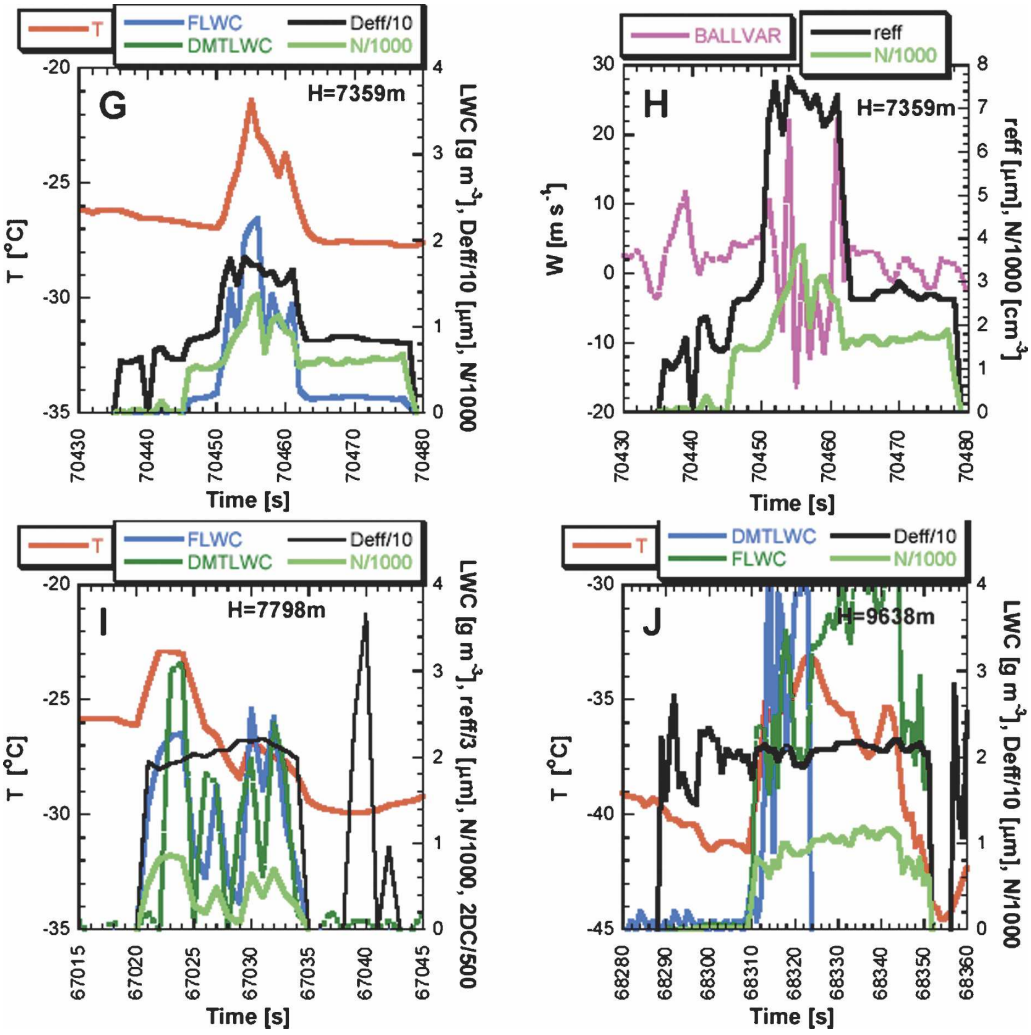

FIG. 12. (*Continued*)

and it is not surprising that some of them produced giant hailstones. To minimize the chances of flying into hailstones, the aircraft penetrated these violent convective towers at not more than about 1000 m below their tops. This fact means that the cloud tops were well exposed to viewing from satellites and that the aircraft measurements are highly relevant to satellite measurements of the vertical evolution of cloud microstructure using the method of Rosenfeld and Lensky (1998; also Rosenfeld and Woodley 2003). Even with this flight precaution, the aircraft still encountered small hailstones and large graupel in the tops of the severe convective elements on 7 February 2000. These ice particles broke the DMT LWC hot-wire, as evidenced by the discontinued DMT LWC measurement in the penetration shown in Fig. 12J.

The vigorous updrafts at temperatures below the threshold of homogeneous freezing appear to have

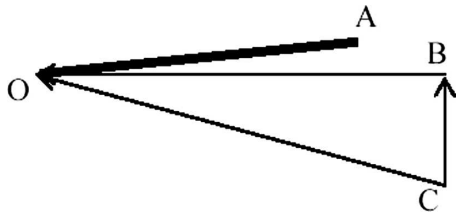

FIG. 13. A schematic illustration of the airflow with respect to the aircraft wing upon entering the updraft. The aircraft wing is represented by the thick line AO, moving horizontally from left to right. The horizontal component of the airflow with respect to the wing is represented by the arrow BO. The angle of attack in vertically still air would then be given by BOA. Upon entering the updraft, before the added forces had time to change the attitude and flight path of the aircraft, the updraft can be represented as an addition of vector CB, resulting in a net relative flow represented by vector CO. The angle of attack would then grow from BOA to COA. A stall would occur when the updraft CB increases to the extent that angle COA grows beyond the critical angle.

been composed of mainly homogeneously frozen cloud drops, as suggested by the similarity of D_{eff} for the water and ice clouds at the same level (see Figs. 11J,L). However, when full heterogeneous glaciation occurred at warmer temperatures, the true D_{eff} of the ice cloud increased well beyond the true D_{eff} of the water or mixed phase cloud at the same level (see Fig. 11F). In ice clouds with large nonspherical particles, the FSSP measures random noise that maximizes at the middle bins. This is manifested as a much larger indicated D_{eff} than that of the water clouds at the same level in these particular clouds. This is evident in the larger indicated D_{eff} of heterogeneously glaciated cloud relative to the D_{eff} of a homogeneously frozen one. In specific terms, the heterogeneous glaciation occurring at the warmer temperatures takes place in a mixed-phase cloud, where the ice particles can continue growing by accretion and by vapor deposition at the expense of the water cloud droplets. Therefore, in addition to the increased D_{eff} due to large ice particles, the droplet concentrations should be lower in heterogeneously glaciating clouds, especially when glaciating at higher temperatures at which freezing of individual cloud droplets is less probable. The FSSP LWC in glaciated clouds corresponds to cloud ice water content, but the relation between this quantity and the true water value is underestimated by an unknown amount.

e. Development of precipitation-sized (>100 μm in diameter) hydrometeors

The 2DC imaging probe was used to examine the precipitation-sized (>100 μm in diameter) hydrometeors during each pass through the vigorous cloud towers. Virtually no precipitation particles were evident at altitudes <8 km. At 150 m s^{-1}, the sample volume of the 2DC probe is approximately 7.3 L s^{-1}. A few images at higher altitudes (colder temperatures) on 1 February 2000 are provided in Fig. 14. The swath width in each of the six panels is 0.8 mm. The coded time provided in each panel corresponds to the times on the abscissa of the panels in Fig. 11. An assortment of ice particles is evident in the images, ranging from <0.1 mm in diameter to 3 mm. The images in Figs. 14C–E at t from 74 350 to 74 352, respectively, show a short image sequence of passage through a small near-adiabatic cloud filament just below the homogeneous freezing point, as shown in Fig. 11I. Small concentration of very small graupel appeared in the core, with larger graupel of a few millimeters at the fringes. Somewhat larger and more numerous graupel were observed in another half-adiabatic LWC core at temperature $T = -36$°C (t = 74 352 in Fig. 14E). Graupel of up to 3 mm appeared in glaciated cores below ($T = -34$°C, t = 73 986 in Figs. 14A and 11H) and above ($T = -45$°C, t = 74 461 in Figs. 14F and 11J) the homogeneous freezing isotherm level. The importance of these observations is with the documentation of cloud parcels that maintained most of their water up to the homogeneous freezing level. Such images under the conditions for which they were obtained are unique in showing how precipitation is initiated in these highly supercooled and microphysically continental clouds, which form the very high "first echoes" that are shown in the next section.

5. First-echo heights

The lack of aircraft-observed precipitation-sized hydrometeors in detectable concentrations (e.g., 0.1 L^{-1} for 1-mm graupel) in the growing convective elements implies a first-echo height above that level. The radar first-echo tops, as observed on 1 and 7 February 2000, were around 8–9 km. A simple unambiguous example of first-echo height was done on 30 January 2000 on an isolated cumulus congestus cloud that formed 75 km northeast of the radar and was clearly visible to the meteorologist (T. Krauss) at the radar site. According to Fig. 8, the cloud microstructure on that day was similar to that of the more fully documented cases on 1 and 7 February 2000. The radar first echo and a photograph of the cloud are shown in Fig. 15. The striking feature is that the cloud appeared to be vertically developed and vigorous but without a significant radar echo. Close observation showed that the cloud base was free of precipitation. The first echo of 20 dBZ appeared at an altitude of 9 km MSL. The radar echo intensified quickly to 51 dBZ in 15 min, as seen in the radar scan of 2300 UT. The cloud photograph for that time shows visible signs of glaciation at the top, a darker cloud base, and the first signs of precipitation. The fact that this relatively moderate and isolated cloud developed such a high first echo suggests that other factors in addition to strong updrafts delayed the precipitation initiation in the clouds. These additional factors can be the relatively high and cold cloud base (cloud-base temperature of 7.5°C at 3.2 km MSL) and the microphysically continental aerosols, leading to nucleation of large concentrations of small droplets with a narrow spectrum at cloud base. It is unfortunate that no CCN measurements were available.

The first echo shown in Fig. 15 is consistent also with the plot of cloud buoyancies ($T_c - T_a$, where the subscripts c and a indicate cloud and ambient, respectively) obtained in vigorous Mendoza convective clouds on four flight days (27 and 28 January and 1 and 7 February) in 2000 (Fig. 16). The maximum supercooled liquid

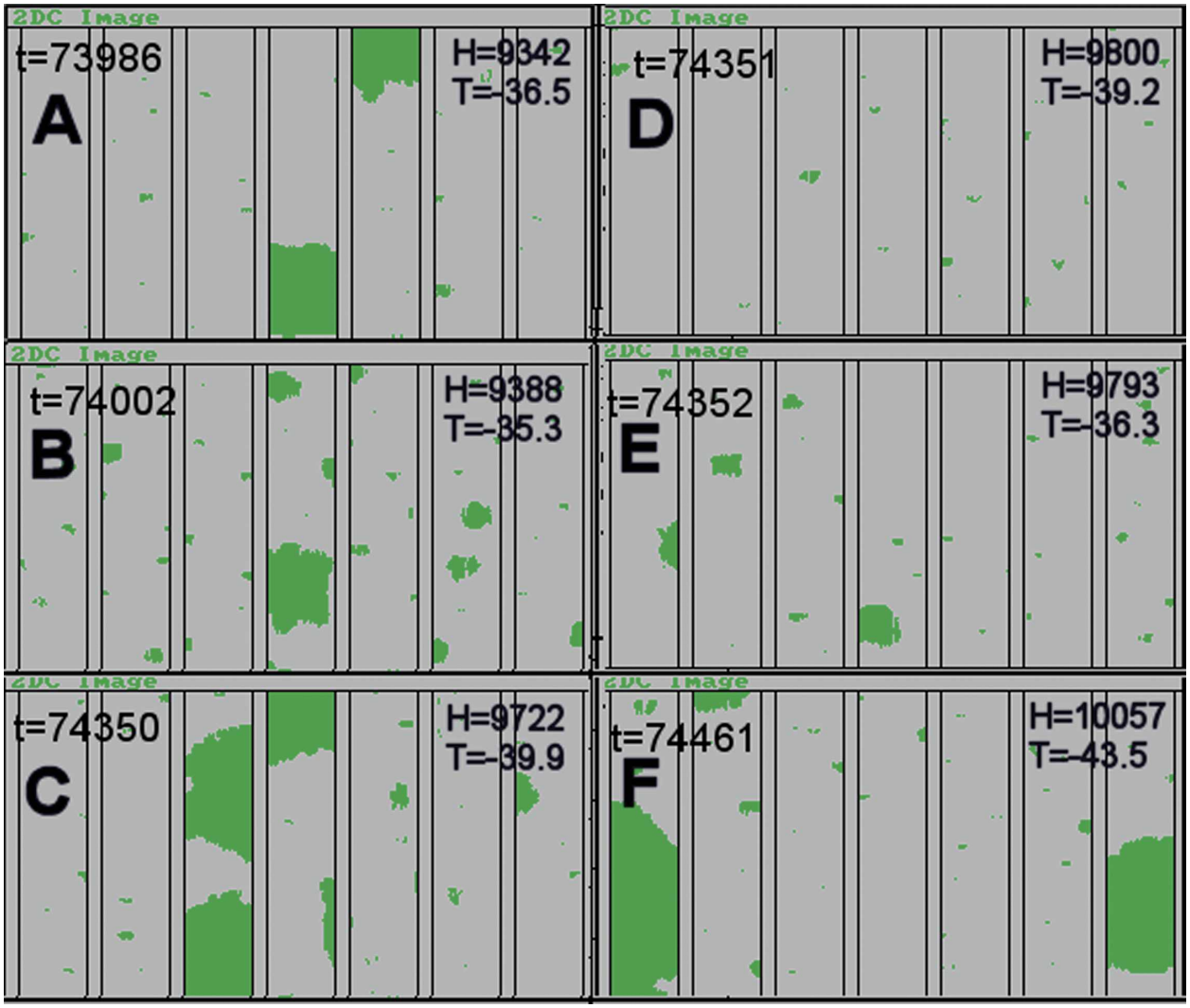

FIG. 14. Images of cloud hydrometeors observed during penetrations of (B), (D), (E) very highly supercooled clouds, (C) mostly glaciated clouds, and (A), (F) fully glaciated clouds on 1 Feb 2000 as shown in Fig. 11. The image slice width is 0.8 mm. The coded time provided in each panel corresponds to the times on the abscissa of the panels in Fig. 12. Note the existence of very few and small hydrometeors in the near-adiabatic cloud segment of (D) and (E), where according to Fig. 11I T peaks at -36°C and LWC peaks at 3 g m^{-3}.

water content (SLWC) and in-cloud temperature of each cloud pass are plotted. The diagonal line denotes the line of zero buoyancy. The horizontal line is the homogeneous freezing temperature of the cloud droplets. It is likely that the coldest first-echo temperatures were produced in the clouds with greatest buoyancies and updrafts. Such clouds are the most troublesome because they provide the smallest lead time between first echo and the existence of fully vertically developed cumulonimbus capable of producing hail, making it difficult to issue timely warnings before the hail potentially begins. They are troublesome also because these are the clouds with strongest updrafts and hence the clouds with the potential of producing the largest hail and the most damage.

6. Discussion

The authors are not aware of any publications documenting the microstructure of hailstorm clouds from cloud base to -45°C. To be specific, the amount of documented highly supercooled liquid cloud water and the thermal buoyancies are the largest that the authors have found in the published literature so far.

The combination of the following conditions observed in the measured clouds constitutes the potential for severe hailstorms:

1) microphysically continental cloud microstructure, having little coalescence and warm rain with the formation of only a few precipitation embryos at low levels,

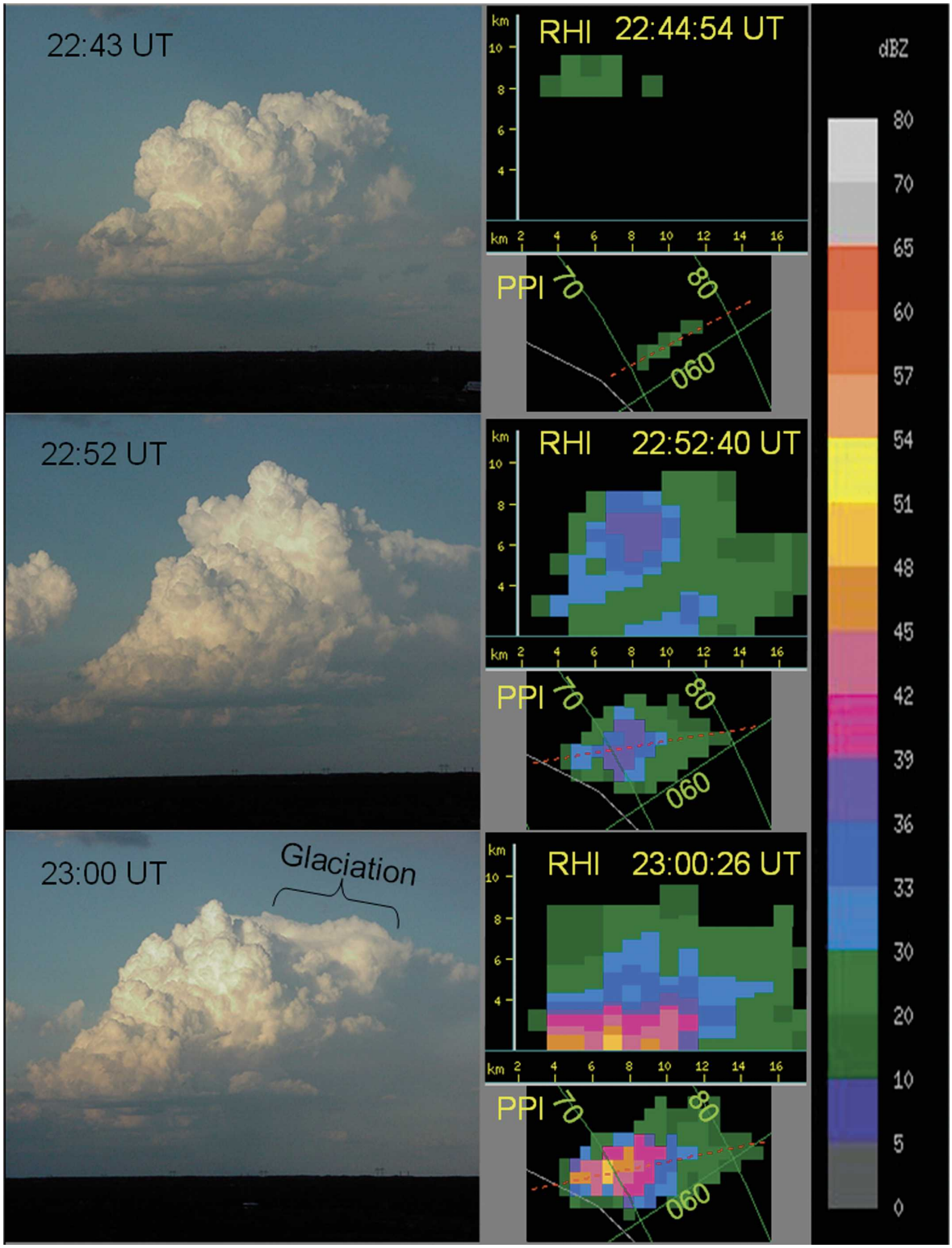

FIG. 15. The formation of precipitation from a first echo in an isolated relatively small cloud on 30 Jan 2000, as documented by the radar and corresponding cloud photograph taken from the radar site. The cloud was centered near 75 km from the radar at an azimuth of 055°. For each radar scan the composite plan position indicator (PPI) of the greatest reflectivity at any height is indicated. The vertical cross section along the red line in each PPI is presented in the range–height indicator (RHI). The RHI frames are 18 km horizontally by 10 km in the vertical direction. The RHI show that the first echo occurred at a height of about 9 km. Cloud base is at a height of 3.2 km above sea level at a temperature of 7.5°C.

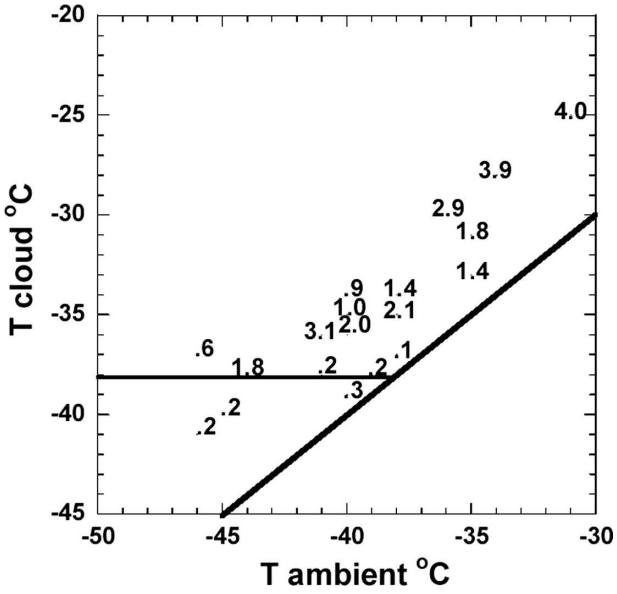

FIG. 16. Observed buoyancies in vigorous Mendoza convective clouds on 27 and 28 Jan and 1 and 7 Feb 2000. The maximum SLWC (g m^{-3}) and in-cloud temperature of each cloud pass are plotted. The diagonal line denotes the line of zero buoyancy, i.e., equal in-cloud and ambient temperatures. The horizontal line is the homogeneous freezing temperature of the cloud droplets. Note that the SLWC generally increases for greater thermal buoyancy, which is given by the distance above the diagonal line, but only at in-cloud temperatures higher than −38°C, as denoted by the horizontal line. The contrast of SLWC at high thermal buoyancy above and below the −38°C line supports the suggestion of homogeneous freezing occurring near this temperature.

2) little loss of cloud water to warm rain and glaciation, leading to a very deep layer of supercooled cloud, containing nearly adiabatic water contents in extreme cases,
3) existence of large amounts of cloud liquid water in the strong updrafts up to the −35°C isotherm with filaments of undiluted and unfrozen updrafts reaching the level of homogeneous freezing near −38°C (this extends the zone of growth of large hailstones upward to that highest possible level),
4) very strong updrafts in the highly supercooled parts (from −25° to −38°C) of the cloud of at least 40 m s^{-1} [such an updraft can support a hailstone with a diameter of 6.0 cm at a temperature of about −25°C (Macklin 1977)], and
5) strong vertical wind shear to separate the updraft from the downdraft, leading to long-lived cell circulations and potential for recirculation of hydrometeors, which has been shown to be a mechanism involved in the formation of large hail (Foote 1984, 1985).

The combination of these conditions can create large (i.e., >3 cm) hail, which was observed from the storms in which the measured clouds acted as feeders. Cloud electrification is the result of collisions between graupel and ice crystals in supercooled clouds, with greater charging at colder temperatures. The enhanced vigor of the storm results in a deeper mixed-phase zone and hence could result in greater charging as well as greater vertical transport of the separated charges. However, the observations that the very strong updrafts delay the onset of mixed-phase processes to the very high levels or even prevent them altogether may lead to the suppression of lightning through a lack of graupel and ice crystal collisions within the cores of such updrafts. There is presently no objective measure of this effect, but lightning discharges were not visibly observed in the vigorous, young, growing, cloud towers that were penetrated during the Argentine cloud-physics campaign. Although it might be ascribed to chance in such a short research effort, the lack of encounters with lightning during the 6 years of operational seeding of such convective elements (R. Tilbury, the seeder pilot of the Learjet, 2004, personal communication) cannot reasonably be ascribed to chance. Similar observations of weak electrical charging in the intense updraft cores of severe storms in the U.S. high plains was reported by Lang et al. (2004), which suggests that the measured clouds in this study possess properties of the core updrafts of severe hailstorms. In contrast, occasional lightning was encountered in the feeders of much less severe and less continental storms, such as in Israel winter thunderstorms over the east Mediterranean region, as experienced by the first author (who also conducted the research flights in Argentina).

It is suggested that severe hailstorms in a microphysically continental air mass have very low precipitation efficiency because much of the cloud water escapes through the anvil during homogeneous freezing or is evaporated because of the small sizes of the hydrometeors other than the low concentrations of the large hailstones.

7. Conclusions

The structures of severe convective storms at high altitudes and low temperatures in Mendoza, Argentina, have been documented for the first time, using a cloud-physics jet aircraft and radar, satellite, and rawinsonde observations. The main research goal was the description of the microphysical evolution of the convective feeders to the storms from cloud base to the anvil cloud tops for obtaining insights to the microstructure of these hail-prone clouds. This was achieved by flying the aircraft preferentially through the young, growing, convective elements, which were typically the major feeders to severe hailstorms, producing large (i.e., >3 cm)

hail. Cloud bases ranged typically between 6° and 14°C, with typical base updrafts of 4–7 m s^{-1}. The cloud updrafts increased with height, exceeding 25 m s^{-1} at heights ≥7 km and occasionally 40 m s^{-1} at heights >8 km. Such updraft speeds will support hailstones that are roughly 6 cm in diameter. Thermal buoyancies of 5°–8°C, which drove the extreme updrafts, were measured in the convective towers at heights of 8–10 km. The vertical wind shear was weak below 6 km but increased strongly above that level as the west winds cleared the Andes barrier, which averages 6.1 km to the west of Mendoza. The clouds had very little coalescence and contained no discernible precipitation-sized particles >100 μm in diameter at $T > -15$°C. Nearly adiabatic cloud water with most cloud water still not converted into precipitation was maintained in some cloud portions within the strongest updrafts up to the level of homogeneous freezing, reaching 4 g m^{-3} at −38°C in one cloud before vanishing abruptly at colder temperatures. Graupel >1 mm appeared at the tops of growing new towers at temperatures of less than −27°C, in agreement with radar first-echo heights of about 8 km. A few isolated frozen raindrops were also observed there.

The complementary information obtained from rawinsondes reinforced these findings. Calculations that use atmospheric soundings as input gave maximum updraft speeds (51–66 m s^{-1}) that exceeded those observed. First-echo tops were noted at 8–9 km, and these were followed by hail formation in as little as 15 min. The aircraft measurements documented intense supercooling of the cloud water to near the point of homogeneous nucleation, indicating a vast reservoir of supercooled water available for the growth of large hailstones.

Acknowledgments. We thank Mr. Pat Sweeney, president of WMI, for supporting this research effort. We are deeply grateful also to Mr. Roger Tilbury, who skillfully and safely piloted the Learjet through the tops of the most vigorous convective cores of the violent hailstorms, resulting in this unique set of observations. Our thanks are also given to Mr. Tilbury for measuring and providing the angle-of-attack estimates necessary for calculating the peak updrafts in the clouds, which exceeded 40 m s^{-1}. This research was supported through the contract between WMI and the Ministry of Economy of the government of Mendoza, Argentina.

REFERENCES

Andreae, M. O., D. Rosenfeld, P. Artaxo, A. A. Costa, G. P. Frank, K. M. Longo, and M. A. F. Silva-Dias, 2004: Smoking rain clouds over the Amazon. *Science,* **303,** 1337–1342.

Barge, B. L., and F. Bergwall, 1976: Fine scale structure of convective storms associated with hail production. Atmospheric Science Division, Alberta Research Council, Edmonton, Rep. 76-2, 43 pp.

Baumgardner, D., and M. Spowart, 1990: Evaluation of the forward scattering spectrometer probe. Part III: Time response and laser inhomogeneity limitations. *J. Atmos. Oceanic Technol.,* **7,** 666–672.

Chisholm, A. J., 1970: Alberta hailstorms: A radar study and model. Ph.D. thesis, McGill University, 287 pp.

——, and J. H. Renick, 1972: The kinematics of multicell and supercell Alberta hailstorms. Alberta Hail Studies: 1972, Research Council of Alberta Rep. 72-2, 24–31.

Dixon, M., and G. Wiener, 1993: TITAN: Thunderstorm Identification, Tracking, Analysis, and Nowcasting—A radar-based methodology. *J. Atmos. Oceanic Technol.,* **10,** 785–797.

English, M., 1986: The testing of hail suppression hypotheses by the Alberta Hail Project. Preprints, *10th Conf. on Weather Modification*, Arlington, VA, Amer. Meteor. Soc., 72–76.

Foote, G. B., 1984: The study of hail growth utilizing observed storm conditions. *J. Climate Appl. Meteor.,* **23,** 84–101.

——, 1985: Aspects of cumulonimbus classification relevant to the hail problem. *J. Rech. Atmos.,* **19,** 61–74.

Freud, E., D. Rosenfeld, M. O. Andreae, A. A. Costa, and P. Artaxo, 2005: Observed robust relations between CCN and vertical evolution of cloud drop size distributions in deep convective clouds. *Atmos. Chem. Phys. Discuss.,* **5,** 10 155–10 195.

Heymsfield, A. J., L. M. Milosevich, C. Schmitt, A. Bansemar, C. Twohy, M. R. Poellot, A. Fridlind, and H. Gerber, 2005: Homogeneous ice nucleation in subtropical and tropical convection and its influence on cirrus anvil microphysics. *J. Atmos. Sci.,* **62,** 41–64.

Knollenberg, R. G., A. J. Dascher, and D. H. Huffman, 1982: Measurements of the aerosol and ice crystal populations in tropical stratospheric cumulonimbus. *Geophys. Res. Lett.,* **9,** 613–616.

Krauss, T. W., and J. D. Marwitz, 1984: Precipitation processes within an Alberta supercell hailstorm. *J. Atmos. Sci.,* **41,** 1025–1034.

Lang, T. J., and Coauthors, 2004: The Severe Thunderstorm Electrification and Precipitation study. *Bull. Amer. Meteor. Soc.,* **85,** 1107–1125.

Lawson, R. P., L. J. Angus, and A. J. Heymsfield, 1998: Cloud particle measurements in thunderstorm anvils and possible weather threat in aviation. *J. Aircr.,* **35,** 113–121.

Macklin, W. C., 1977: The characteristics of natural hailstones and their interpretation. *Hail: A Review of Hail Science and Hail Suppression, Meteor. Monogr.*, No. 38, Amer. Meteor. Soc., 65–88.

Makitov, V., 1999: Organization and main results of the hail suppression program in the northern area of the province of Mendoza, Argentina. *J. Weather Modif.,* **31,** 76–86.

Marwitz, J. D., 1972a: The structure and motion of severe hailstorms. Part I: Supercell storms. *J. Appl. Meteor.,* **11,** 166–179.

——, 1972b: The structure and motion of severe hailstorms. Part II: Multicell storms. *J. Appl. Meteor.,* **11,** 180–188.

——, 1972c: The structure and motion of severe hailstorms. Part III: Severely sheared storms. *J. Appl. Meteor.,* **11,** 189–201.

Musil, D. J., and P. L. Smith, 1986: Aircraft penetrations of Swiss hailstorms: An update. *J. Weather Modif.,* **18,** 108–111.

——, A. J. Heymsfield, and P. L. Smith, 1986: Microphysical char-

acteristics of a well-developed weak-echo region in a high plains thunderstorm. *J. Climate Appl. Meteor.,* **25,** 1037–1051.

——, S. A. Christopher, R. A. Deola, and P. L. Smith, 1991: Some interior observations of southeastern Montana hailstorms. *J. Appl. Meteor.,* **30,** 1596–1612.

Rosenfeld, D., and I. M. Lensky, 1998: Spaceborne sensed insights into precipitation formation processes in continental and maritime clouds. *Bull. Amer. Meteor. Soc.,* **79,** 2457–2476.

——, and W. L. Woodley, 2000: Convective clouds with sustained highly supercooled liquid water down to −37.5°C. *Nature,* **405,** 440–442.

——, and ——, 2003: Closing the 50-year circle: From cloud seeding to space and back to climate change through precipitation physics. *Cloud Systems, Hurricanes, and the Tropical Rainfall Measuring Mission (TRMM): A Tribute to Dr. Joanne Simpson*, *Meteor. Monogr.,* No. 51, Amer. Meteor. Soc., 59–80.

Smith, P. L., J. L. Stith, and D. A. Barrows, 1994: Observations of microphysical evolution in a high plains thunderstorm anvil. *Atmos. Res.,* **33,** 25–35.

Tsonis, A. A., W. R. Leaitch, and M. D. Couture, 1987: The effect of calibration of the forward-scattering spectrometer probe on the sizing of cloud droplets. *J. Atmos. Oceanic Technol.,* **4,** 518–526.

World Meteorological Organization, 1995: WMO meeting of experts to review the present status of hail suppression. WMO Tech. Doc. 764, 39 pp.